Composite Structures 301 (2022) 116139

Contents lists available at ScienceDirect

Composite Structures

journal homepage: www.elsevier.com/locate/compstruct

Experimental study of the high-power laser resistance of ablative material-filled sandwich panels with truss cores under hypersonic airflow

Wu Yuan [a,b], Jiangtao Wang [a,b], Ruixing Wang [a,b], Zhe Wang [a,b], Hongwei Song [a,b,*], Chenguang Huang [b]

[a] Key Laboratory for Mechanics in Fluid-Solid Coupling Systems, Institute of Mechanics, Chinese Academy of Sciences, Beijing 100190, China
[b] School of Engineering Sciences, University of Chinese Academy of Sciences, Beijing 100049, China

ARTICLE INFO

Keywords:
Laser resistance
Sandwich panel
Thermal insulation
Lightweight structure
Failure point

ABSTRACT

In this study, the performance of ablative material-filled sandwich structures with truss cores under laser irradiation is experimentally analyzed in a hypersonic wind tunnel. As a comparison, we investigated the responses of a monolithic high-temperature alloy plate, unfilled sandwich panel, and thermal insulating material-filled sandwich panel. Failure times and ablation morphologies are assessed using a high-speed camera, while temperature histories are obtained using a colorimetric pyrometer. Experimental results show that, when subjected to a transverse hypersonic airflow, the laser resistance of the ablative material-filled sandwich structures is substantially better than that of other structures. Compared to a static environment, failure times of the sandwich structures in the hypersonic airflow are reduced due to the mechanical erosion effect. The detailed action mechanisms of the ablative material-filled sandwich structures are revealed by numerical modeling and the characterization of the ablation morphology.

1. Introduction

With the development of high-power lasers, laser-resistant performance became a crucial concern in the design of high-speed aircraft. The local intense heat flux induced by a continuous-wave (CW) laser may result in uncontrollable damage of inner parts after the frontside surface is burned through. Various materials and structures were investigated to alleviate laser-induced damage. The application of reflecting materials is very promising for the reduction of the absorbed laser power by increasing the surface reflectivity of the respective structures [1]. However, the occurrence of impurities during the service life or in the preparation process critically deteriorates their functional properties, and high reflectivity is only satisfied for a CW laser at a specific wavelength. Ablation-type materials used in the thermal protection systems react to the absorbed laser power by pyrolysis and phase change of the composite material, which is another way to reduce the laser damage [2]. Besides, diffusion materials and composite laser protection systems can be also used for structures that undergo CW laser irradiation [3].

Recently, we proposed that filled sandwich structures have superior performance when irradiated with a high-power laser. In the static air environment, the CW laser resistance of ablative material-filled sandwich panels with truss cores (A-SPTC) is superior to that of monolithic plates, sandwich panels with truss cores (SPTC), and thermal insulation material-filled sandwich panels with truss cores (I-SPTC) at a same areal density. The mechanisms of the laser resistance and ablation process are determined by the analysis of the laser ablation residue and three-dimensional numerical modeling [3,4]. However, in a normal working environment, sandwich structures used in airplanes are always exposed to an adverse hypersonic airflow, so the performance of these structures under the coupled effect of hypersonic airflow and high-power CW laser is of utmost importance. Besides, due to their superior performance in load bearing [5–7], sound absorption [8], energy absorption [9–11], damping efficiency [12], and high designability [13,14]. Sandwich structures with truss cores can be also extensively used in integrated thermal protection systems (ITPS) of aerospace industries. A thermal-resistant structure with favorable performance under the irradiation of high-power laser has a high practical significance in engineering.

During high-speed flights, the influence of the airflow on the performance of structures irradiated by a CW laser is not trivial. Johnson et al [15] developed an interpolation formula to calculate the laser burn

* Corresponding author at: Key Laboratory for Mechanics in Fluid-Solid Coupling Systems, Institute of Mechanics, Chinese Academy of Sciences, Beijing 100190, China.
E-mail address: songhw@imech.ac.cn (H. Song).

https://doi.org/10.1016/j.compstruct.2022.116139
Received 9 March 2022; Received in revised form 17 June 2022; Accepted 13 August 2022
Available online 28 August 2022

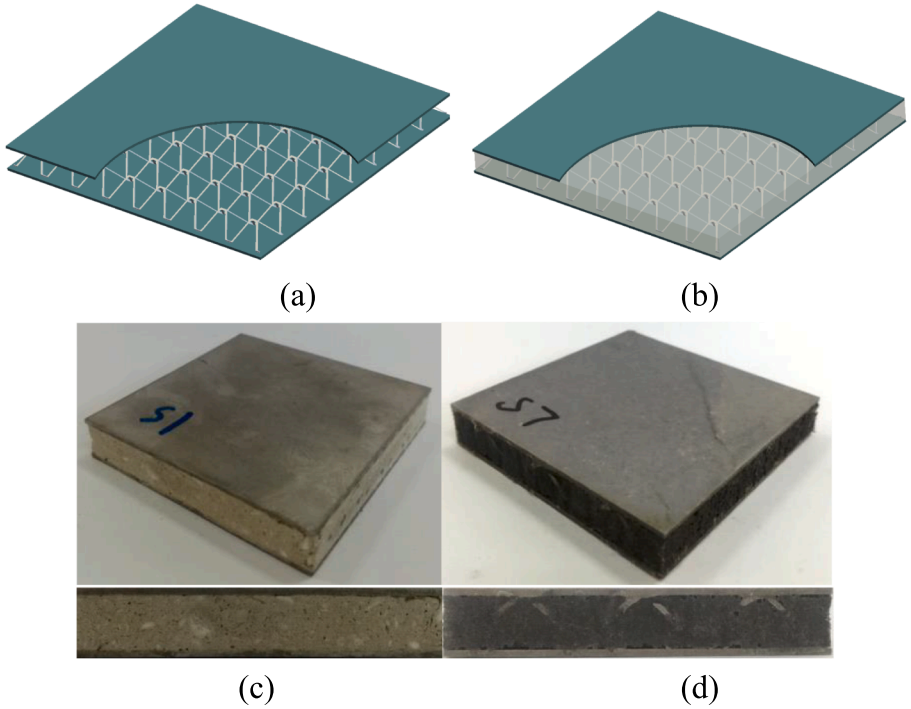

Fig. 1. The fabricated specimen. (a) schematic of the unfilled SPTC, (b) schematic of the filled SPTC, (c) ablative material-filled SPTC, (d) thermal insulation material-filled SPTC.

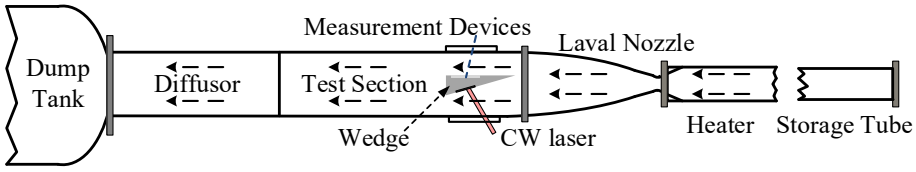

(a) The hypersonic wind tunnel.

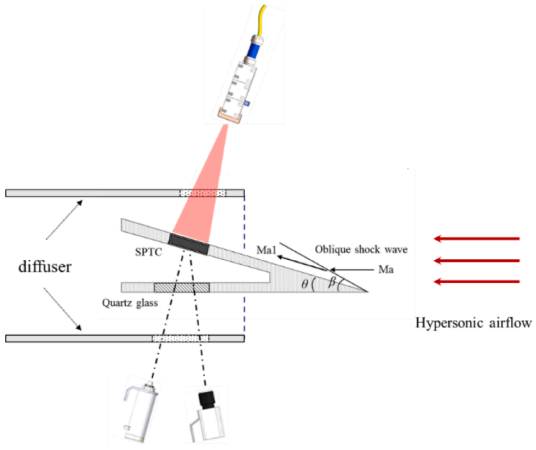

(b) The layout of the wedge and equipment of the laser ablation test.

Fig. 2. Schematic of the laser irradiation experimental setup: (a) the hypersonic wind tunnel and (b) the layout of the wedge and equipment of the laser ablation test.

through time reduction due to the tangential airflow. O'Keefe et al [16] gave theoretical results of laser melt through time reduction due to aerodynamic melt removal. Crane et.al [17] gave the mechanisms of melt removal for specimen with different materials subjected to laser radiation and low-speed gas flows. By using the numerical methods, Huang et.al [18] and Marineau et al [19] studied the laser ablation behavior of composite materials under supersonic airflow. Baumann et. al [20] investigated the fiber laser heating and penetration of aluminum in shear flow experimentally. Wang et al [21] presented experimental results for laser ablation behavior of C/SiC composites under supersonic airflow. In conclusion, the tangential airflow to the irradiated surface mainly produces two effects [22]: firstly, it feeds energy into unstable

Table 1
Parameters ahead and behind of the shock wave.

Parameters	Static Temperature (K)	Total pressure (kPa)	Static pressure (kPa)
Ahead shock wave	222.44	4257.06	2.55
Behind shock wave	450.48	2266.65	16.79

Table 2
The list of the used testing parameters.

Specimen	Laser diameter mm	Laser power density W/cm^2	Time on S	Ma	Areal density, g/cm^3
HTA plate	10	1273.8	4	6	2.02
HTA	10	2547.8	4	6	2.02
plate	10	1273.8	4	6	1.61
SPTC	10	2547.8	4	6	1.61
SPTC	10	1273.8	4	6	1.91
I-SPTC	10	2547.8	4	6	1.91
I-SPTC	10	1273.8	4	6	2.00
A-SPTC	10		4	6	2.00
A-SPTC					

surface disturbances [23] which can sometimes even protect the surface via convective cooling [24]; secondly, aerodynamic pressure or shear stress is exerted on the gas/melt interface [25]. For metallic materials, the airflow removes the melted material and the oxide layer, which increases the ablation rate [24]. The decrease of aerodynamic force even causes the rupture of the thin sheets at temperatures notably lower than the melting point [25]. For composite materials, the aerodynamic force of the supersonic airflow induces mechanical erosion, increases the ablation rate, and flattens the ablation surface. In conclusion, the apparent effect of the high-speed airflow on the laser ablation threshold of the specific structure is under the simultaneous and competing influence of aerodynamic force and aerodynamic cooling.

However, the above-mentioned studies were conducted under the high-speed airflow below Mach 5. The aerodynamic heat increases with the cube of the speed, and the aerodynamic force is proportional to the square of the speed. Therefore, the aerodynamic effects of the hypersonic airflow on the CW laser ablation behavior of the filled SPTC are more complex. In the present work, the performance of the A-SPTC under the high-power CW laser is tested in a hypersonic wind tunnel. Failure times and failure modes of the structures under different CW laser powers are obtained using the real-time measuring system and the microstructural analysis of the ablation products after the experiment. Firstly, we introduce the fabrication process of the filled SPTC. Then, we perform a series of laser irradiation experiments on the structures with different configurations in the wind tunnel to analyze the effect of the high-speed airflow, laser power, and structural form. Experimental results show that the performance of the A-SPTC is superior to that of the monolithic plates and other configurations not only in the static airflow environment but also in the presence of the hypersonic airflow.

2. Experiments

2.1. Specimen preparation

Fig. 1 shows the fabrication of the filled SPTC. The pyramidal truss core with a side length of ~ 10 mm is made of a stainless-steel wire mesh. The three-dimensional structures are obtained by the folding method. The cross-section of the truss member is ~ 0.7 mm × 0.9 mm. The relative density of the truss core is ~ 3 %. The truss core and solid facesheets are bonded by using the brazing technique. The side length of the square sandwich panel is 50 mm. The thickness of the truss core and the facesheet are 7 and 0.9 mm, respectively. Four different types of specimens are tested in the experiment for comparison: monolithic high-temperature alloy plate, SPTC, insulation material-filled SPTC (I-SPTC), and ablative material-filled SPTC (A-SPTC). The ablative material is the compound of the silicone resin combined with different carbon powder percentages. The component of silicone resin matrix is Polydimethylsiloxane (PDMS). Spherical carbon particles with diameters of 100 μm −200 μm are uniformly distributed in the PDMS. According to the content of the carbon particles, the densities of ablative material are 0.8 g/cm^3 ~ 1.1 g/cm^3. Detailed Fourier transform infrared spectroscopy, scanning electron microscope and energy dispersive spectrometer of the ablative materials can be found in reference [3]. The component of the insulation material is porous ceramic. The toothpaste-like ceramic putty in the initial state was inserted into the truss core and then solidified at room temperature to form the SPTC with porous ceramic fillers. The densities of ablative material are 0.36 g/cm^3 ~ 0.41 g/cm^3.

The densities of the thermal insulation and ablative materials are 0.48 g/cm^3 and 0.8 g/cm^3, respectively. The thermal insulation and ablative filler materials increase the weight for ~ 17.5 % and 25 % of the

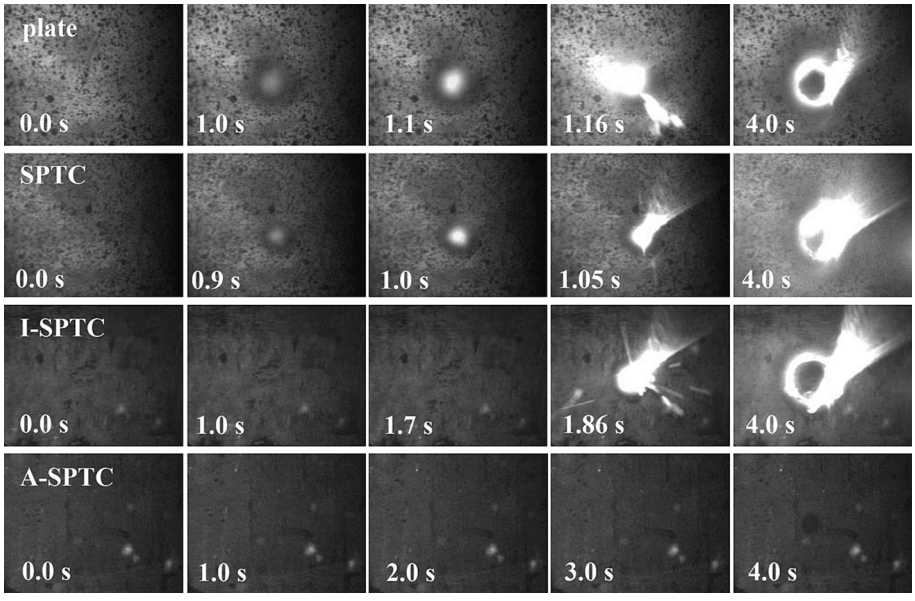

Fig. 3. Failure process of the backside surface for different types of structures recorded by the high-speed camera at the output laser power density of 2547.8 W/cm^2.

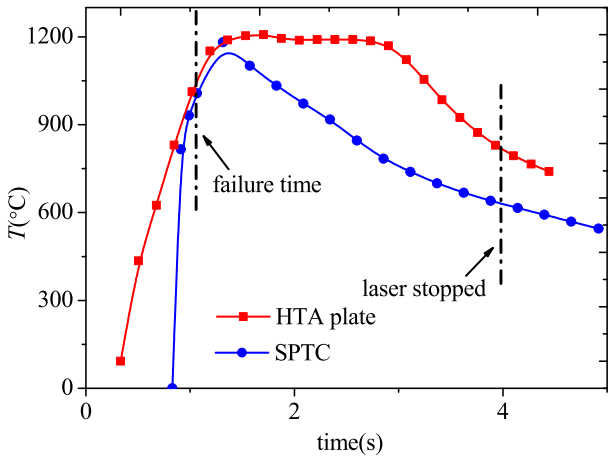

(a)

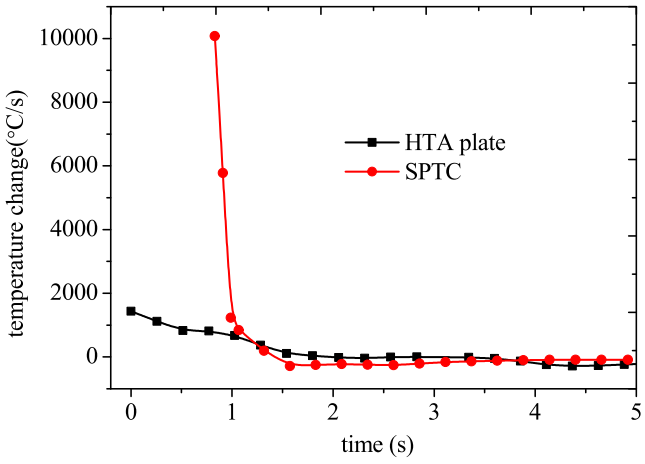

(b)

Fig. 4. Comparison of thermal responses between the monolithic HTA plate and the unfilled SPTC: (a) the temperature and (b) the temperature change.

unfilled SPTC mass, respectively. Monolithic plates with a thickness of 2.4 mm are also fabricated as a comparison.

2.2. Experimental setup

As shown in Fig. 2, laser irradiation experiments on the filled SPTC under the high-speed airflow are performed in a hypersonic wind tunnel facility of Institute of Mechanics, Chinese Academy of Sciences. An IPG YLS 2000 W fiber laser operating at 1.07 μm was utilized as a laser source. The diameter of the laser beam during the wind tunnel experiment is 10 mm, and the distance between the specimen and the laser head is 875 mm. Based on the oxygen-hydrogen combustion, a free-stream of Mach 6 is provided in the test section. The total temperature is 1784 K, and the total pressure is.

4.26 MPa. The measuring system is located on the opposite side of the laser system to monitor the thermal response of the backside surface. The failure time and the failure process are recorded by a high-speed camera with a sampling frequency of 80 Hz and resolution of 1600 × 1200 pixels. A colorimetric pyrometer is used to get the average temperature of the laser diameter on the backside surface of the specimen. To enable the accomplishment of each sequence of the test procedure and the measurement accuracy, we develop the sequential control system of the experimental system based on the Digital Delay Generator Stanford DG535, with a precision of 1 ns.

A wedge model is designed to simulate the service environment of the laser protection system. The wedge has a small rectangle window that replaces the tested specimen. To measure the response of the back surface, we place a heat-resistant quartz glass opposite to the specimen. During the test, the angle of the wedge, θ, is 16°. An oblique shock wave is generated at the tip. Ma and $Ma1$ are Mach numbers ahead and behind of the shock wave, respectively. According to the aerodynamics relations, the shock angle β and $Ma1$ are calculated to be 23.67° and 3.9°, respectively. Detailed parameters are given in Table 1.

As presented in Table 2, the sequences of the areal densities for the four investigated types of structures are: plate, A-SPTC, I-SPTC, and SPTC. The laser irradiation time is 4 s. The output laser power density during the experiment is 1273.8 W/cm^2 and 2547.8 W/cm^2, respectively.

3. Experimental results

3.1. Damage evolution and temperature history

Fig. 3 shows the failure process of the backside surface for the four types of investigated structures recorded by the high-speed camera at a laser power density of 2547.8 W/cm^2. The regions with a high gray value indicate a higher temperature increase induced by the thermal radiation. For the plate, the backside surface has an apparent temperature increases when the laser irradiation time is ~ 1 s. Afterward, the size of the high-temperature region grows rapidly with the irradiation time. Finally, under the combined action of the CW laser and the hypersonic airflow, the plate is burned through at the laser irradiation time of ~ 1.26 s.

Due to the thermal resistance of the truss core, the thermal response time of the backside surface of the SPTC is longer than that of the plate. However, the failure time of the SPTC of 1.04 s is lower than that of the monolithic plate. The comparisons of the average temperature and the temperature difference in the laser spot of the backside surface between the monolithic plate and the SPTC. Fig. 4 reveals that although the SPTC has a longer thermal response time, the temperature difference of the SPTC substantially increases when the frontside of the SPTC is burned through. Therefore, the role of filler in the truss cores is essential.

These results indicate that both the thermal response time and the failure time of the I-SPTC are longer than those for the plate and the SPTC. Compared with the thermal insulation filler material, the processes of pyrolysis, oxidation, and sublimation of the ablative material during the laser ablation require a high amount of absorbed laser energy. Besides, the effects of thermal insulation of intact and degraded materials also increase the time required for the heat flux to reach the backside surface of the filled sandwich structures [3]. Therefore, as shown for the failure process of the backside surface, the performance of the sandwich panel is substantially improved when the truss core is filled with the lightweight ablative material. There is only a little change of the gray value on the image of the backside surface of the A-SPTC even at the laser irradiation time of 4 s. It means that the high-power CW laser does not make notable damage to the inner equipment at these conditions when the A-SPTC structures are used as a protection system.

3.2. Comparison of ablation morphologies

Comparisons of the ablation morphologies among structures with different configurations are shown in Fig. 5. Annular regions around the ablation hole in the inside surface refer to the place which experienced high temperature. The size of the high-temperature region of the monolithic plate is larger than those of the sandwich structures. When the truss core is filled with the thermal insulation material, the size of the thermal response region of the sandwich structure decreases further. Under these conditions, damage induced by the CW laser is negligible

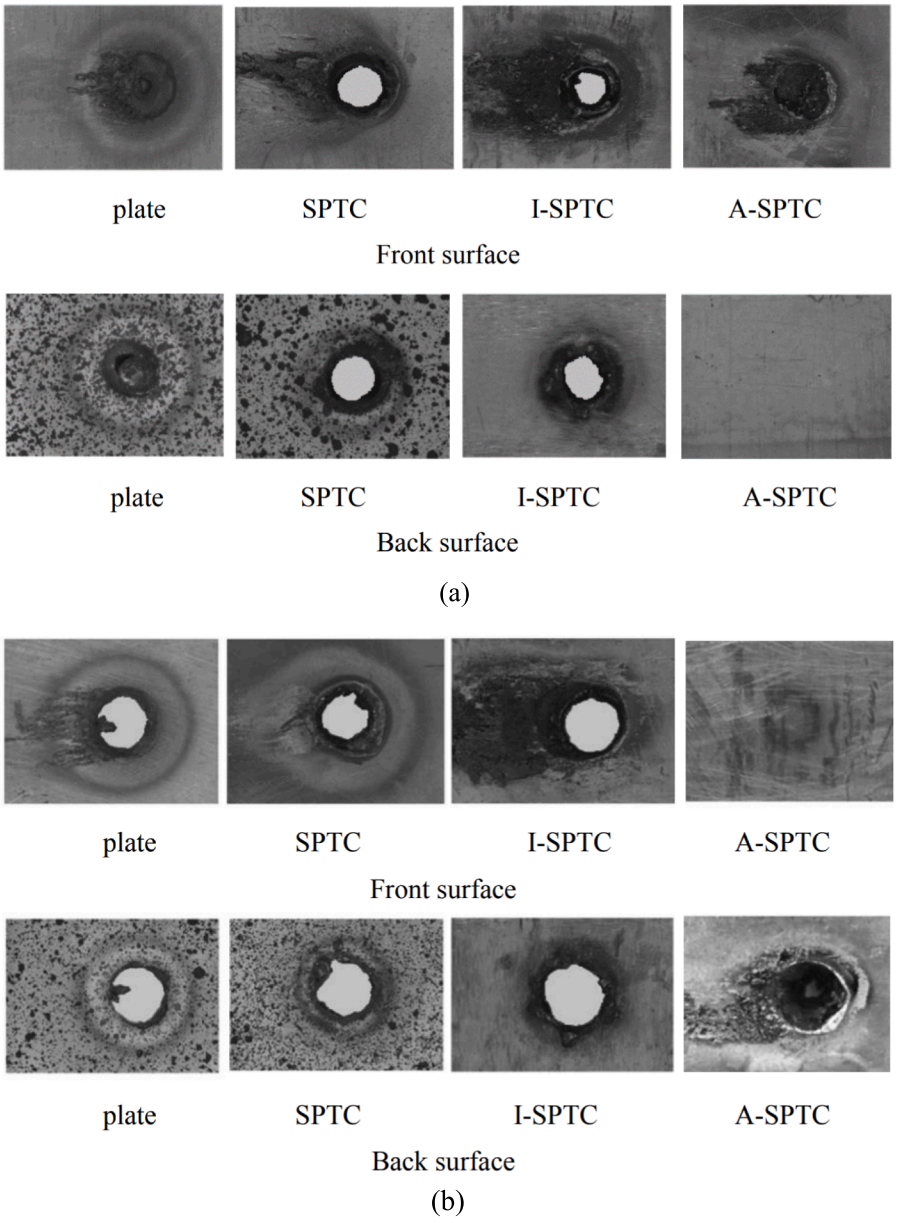

Fig. 5. Ablation morphology of different configurations under the high-speed airflow. (a) laser power density of 1237.8 W/cm^2, (b) laser power density of 2547.8 W/cm^2.

even at a laser power of 2547.8 W/cm^2.

After the hypersonic wind tunnel tests, the full-field ablation depths, and the ablation morphologies of the monolithic plate and the A-SPTC irradiated with the laser power density of 1273.8 W/cm^2 and 2547.8 W/cm^2 are investigated by a HIROX three-dimensional microscope (KH-8700), which is shown in Table 3. Diameters of the ablation hole in the inside surface of the monolithic plates are 0.9 and 4.4 mm when the laser power density are 1273.8 W/cm^2 and 2547.8 W/cm^2, respectively. However, the A- SPTC still shows a respectable CW-laser resistance. The residual thickness, which is defined as the minimum distance between the ablation pit and the inside surface are 0.9 and 6.0 mm respectively. The ablation damage is not found in the backside surface of the SPTC even when irradiated at laser power density of 2547.8 W/cm^2. As previously reported in reference [26], the laser does not only protect the inner equipment but also has a load-bearing capacity at these conditions. Another interesting phenomenon found in the experiment is that the ablation is asymmetric when the ablation thickness increases. As shown in Fig. 6, the ablation pit is symmetric for the monolithic plate but asymmetric for the filled SPTC.

3.3. Comparison of laser resistance performances

Quantitative comparisons of failure times of the four investigated types of structures under the irradiation of a CW laser with different powers are given in Table 4. It should be noted that the tendency of the laser resistance between the plate and the SPTC is different when the laser power is changed. The performance of the plate is superior to the SPTC at a laser power density of 2547.8 W/cm^2, and the failure times are 1.26 and 1.05 s, respectively. However, the failure time of the SPTC is longer than the plate when at a laser power density is decreased to 1273.8 W/cm^2. Thus, the SPTC structure is more suitable as a protection system at lower powers of the CW laser. As shown in Table 4, the performances of the filled SPTC structures, especially the one filled with the ablative material, are superior to the plate and SPTC when the laser power is different.

Comparisons of failure times for the three investigated types of

Table 3
Full-field ablation depths and ablation morphologies of specimens under the hypersonic airflow irradiated by different laser power densities.

ablation depth	ablation morphology
HTA plate, $P = 1273.8$ W/cm^2 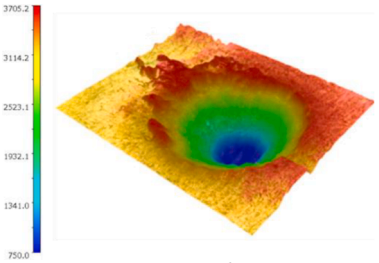	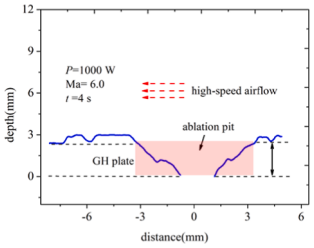
HTA plate, $P = 2547.8$ W/cm^2 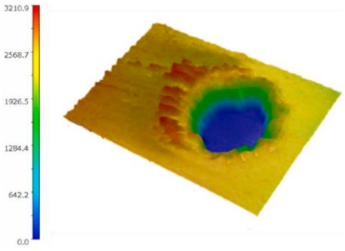	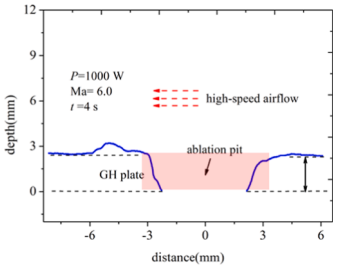
SPTC, $P = 1273.8$ W/cm^2 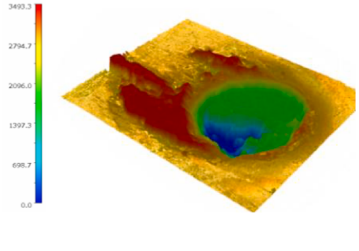	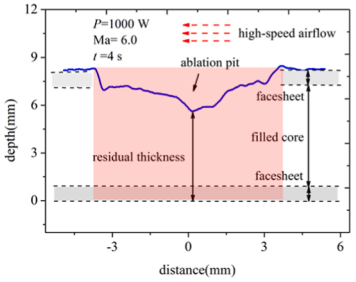
SPTC, $P = 2547.8$ W/cm^2 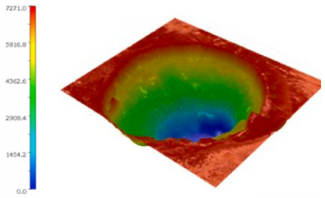	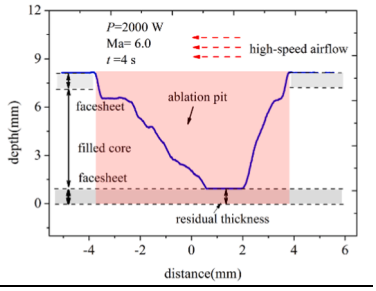

structures irradiated by the CW laser with the power density of 2547.8 W/cm^2 under the static air environment and the hypersonic airflow are shown in Fig. 7. The time required to reach the melting point of the backside surface is defined for structures in the static air experiment as the failure time. For structures in hypersonic airflow, the burn-through time is defined as the failure time. The increment of the threshold of laser damage induced by the hypersonic airflow for the CW-laser induced damage threshold of the investigated structures are 69 %, 77 %, and 70 % for the plate, SPTC and I-SPTC, but less than 34 % for A-SPTC.

4. The mechanism of the hypersonic airflow effect on laser damage

Experimental results show that the hypersonic airflow plays an important role in the laser ablation behavior of all investigated structures. Three important findings can be summarized: (1) laser resistances of the A-SPTCs are superior to other kinds of structures; (2) hypersonic airflow accelerated the ablation; (3) asymmetric ablation is developed when the ablation thickness is increased. Thus, we perform two-dimensional numerical modeling to analyze a detailed mechanism of the effect of the aerodynamic heat and aerodynamic force on the laser resistance of the filled SPTC.

4.1. Numerical model

A numerical two-dimensional model that considers the overall wedge shape and local ablation pit is developed based on the computational fluid dynamics to analyze the effect of the aerodynamic force on the laser ablation behavior of the investigated structures under the hypersonic airflow. Fig. 8 shows the mesh grid of the computational domain. The diameter of the ablation pit is 10 mm and the depths are 1 and 5 mm. The two-dimensional Reynolds-averaged Navier–Stokes (RANS) equations and the SST k–ω turbulence model are employed to

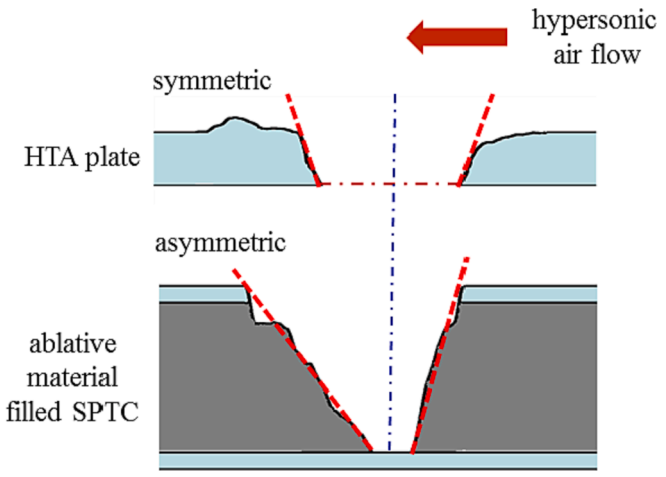

Fig. 6. Symmetry plane of the ablation pit for the HTA plate and the ablative material-filled SPTC.

Table 4
Comparisons of failure times for the four investigated types of structures under high-power laser irradiations with different powers.

Power densities	Environment	HTA plate	SPTC	Insulation material filled SPTC	Ablative material filled SPTC
2547.8 W/cm^2	Hypersonic	1.26 s	1.05 s	1.81 s	> 4 s
	Hypersonic	2.33 s		3.13 s	> > 4 s
1273.8 W/cm^2	Static air	3.77	2.85 s	6.00 s	6.07 s
	Static air	7.70 s		9.40 s	19.5 s
2547.8 W/cm^2			4.70 s		
1273.8 W/cm^2			7.00 s		

simulate the aerodynamic distribution around the ablation cavity. The SST k–ω turbulence model is considered in the numerical model. To accelerate the convergence rate, we used the second spatially accurate upwind scheme with the advection upstream splitting approach flux vector splitting. The Courant–Friedrichs–Levy number is kept at 1. Variables from the interior of the domain are extrapolated to the outlet boundary. The whole model is assumed to have an isothermal temperature of 300 K. The ratio of specific heat is 1.4. Slip wall conditions are bot applied to the viscous surfaces of the model. Thermally and calorically perfect gas and the Sutherland law of viscosity are utilized. The freestream Mach number is 6. Static temperature and static pressure, which are the same as in the wind tunnel experiment, are 222 K and 8550 Pa, respectively.

4.2. Effects of aerodynamic heat

According to the Newton cooling law, the heat flux applied on the ablation pit surface is determined by the difference between the surface temperature, *T*w, and the total temperature of the hypersonic airflow, *T*e, which can be expressed as follows:

$$q_{\text{conv}} = h_w(T_e - T_w) \tag{1}$$

Where h_w is the coefficient of the heat transfer by convection. Compared with laser heat flux, q_{conv} is at least two orders of magnitude less, and can be neglected in this analysis. In the present work, the total temperature of the hypersonic airflow is higher than the melting point of the plate and the stainless steel, which is about 1627 K. The recovery temperature along the surface of the ablation pit is shown in Fig. 9. It can be observed that the aerodynamic heat increases the heat flux on the ablation surface and accelerates the ablation. However, the melting point of the ceramic filler and the sublimation point of the ablation filler, which are ~ 2273 K and 3000 K, respectively, are higher than the total temperature, resulting in the protective effect of the aerodynamic heat on the filled SPTC under these conditions.

4.3. Effects of aerodynamic force

Fig. 10 shows the pressure field and the streamline around the ablation pit obtained by numerical modeling. The mode of cavity flow in the ablation pit varies when the thickness of the ablation increases. As reported in references [27–29], the closed cavity flow occurs for deep cavities. When the ratio of diameter to the depth of the ablation pit L/D

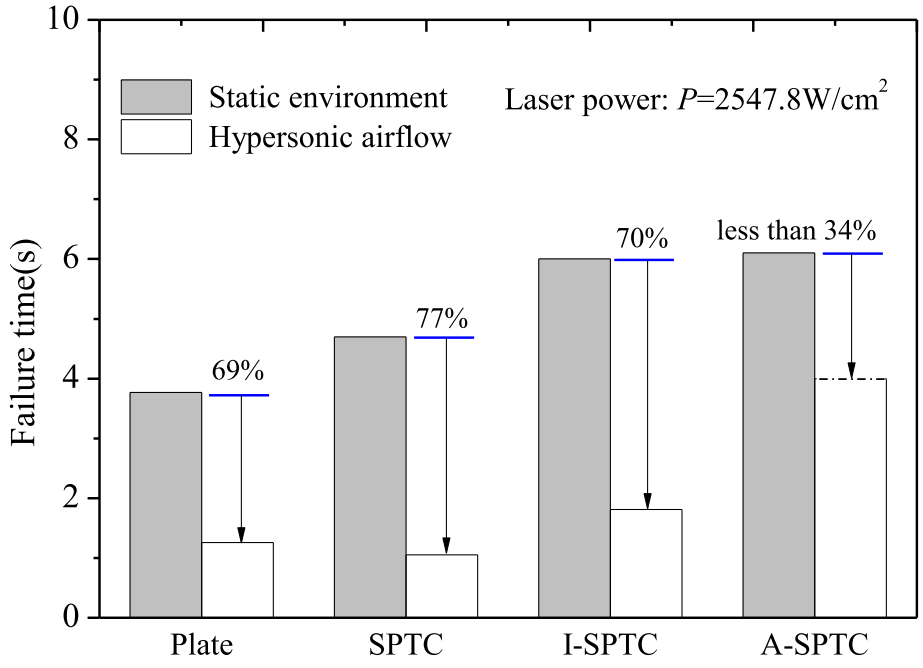

Fig. 7. Comparisons of failure times for the structures with different configurations in the open-air environment and the hypersonic airflow.

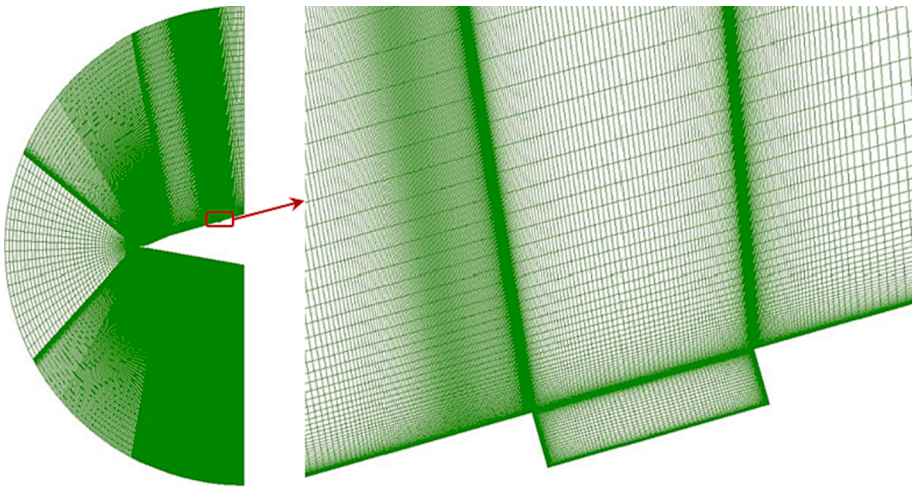

Fig. 8. Mesh grid of the computing domain used in the numerical modeling.

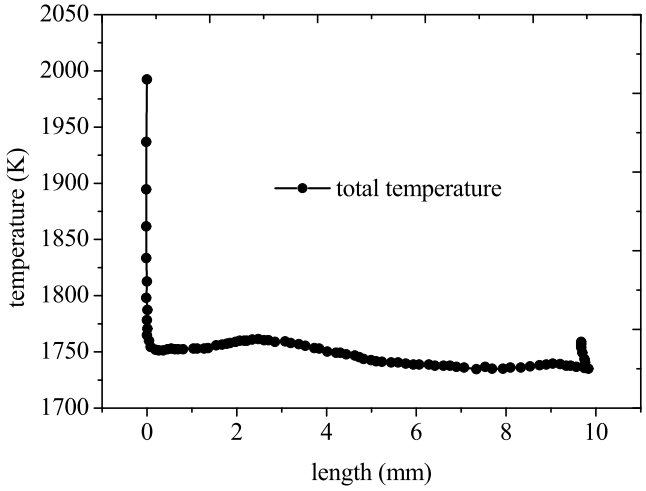

Fig. 9. Recovery temperature along the surface of the ablation pit.

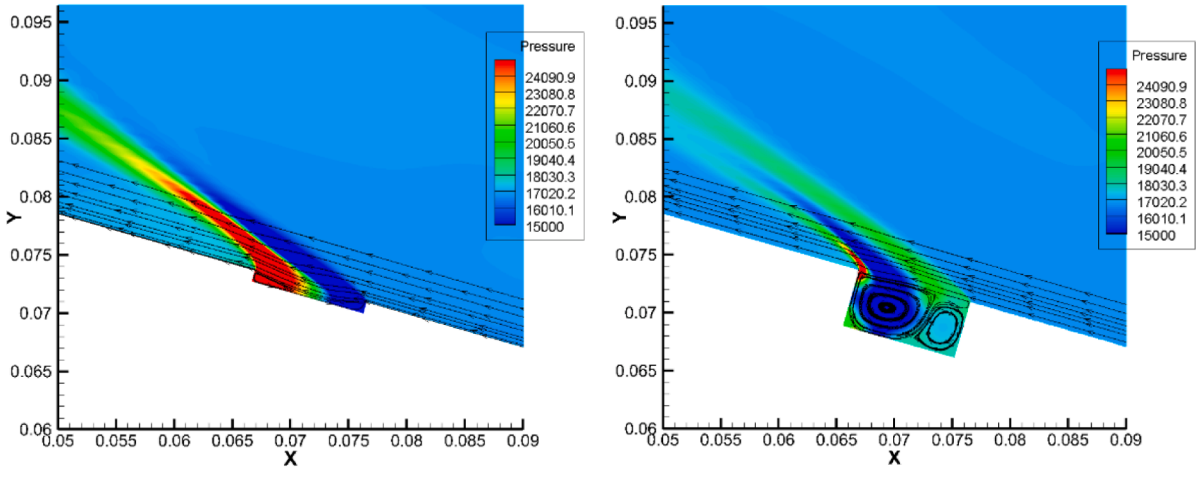

Fig. 10. The CFD results: pressure field and streamlines inside the ablation pit: (a) radius of the ablation pit, r = 5 mm, thickness of the ablation pit, t = 1 mm, and (b) radius of the ablation pit, r = 5 mm, thickness of the ablation pit, t = 5 mm.

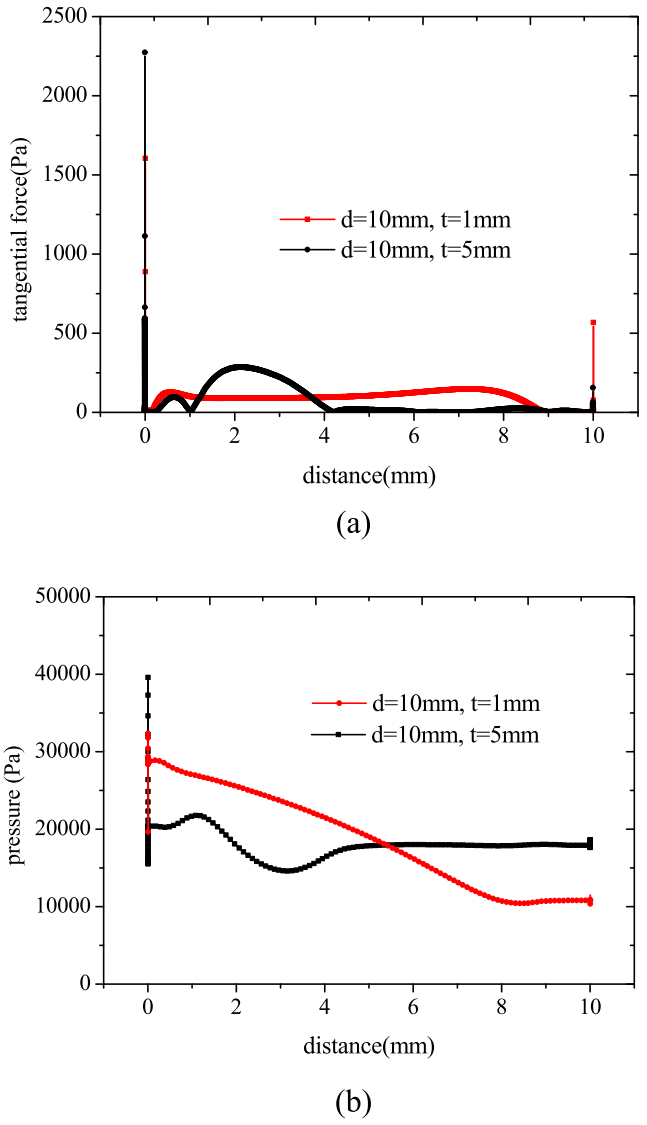

Fig. 11. Aerodynamic force along the wall of the ablation pit: (a) tangential force and (b) pressure.

is decreased, the open cavity flow occurs.

Fig. 11 shows the tangential force and the pressure along the wall of the ablation pit when the thickness increases. The maximal tangential forces exist in the back wall of the ablation pit, being 2.2 kPa and 1600 kPa. Due to the stagnation effect of the front wall, a low-stress zone exists in front of the bottom wall. The size of the low-stress zone increases with the thickness of the ablation pit. As shown in Fig. 11 (b), the static pressure along the wall of the ablation pit is about 10–20 times higher than the tangential stress. When the ablation pit is shallow, the static pressure increases near the right wall. As the laser irradiation time increases, a region with a lower static pressure occurs near the left wall. Therefore, the asymmetric ablation morphology in this region is formed.

4.4. Material characterization

Fig. 12 shows the comparison of ablation morphologies between the A-SPTC tested in the static airflow environment and the hypersonic wind tunnel. In both experiments, the laser power is 1000 W and the diameter of the laser spot is 10 mm. However, the laser irradiation time is about 25 s in the static air environment. As shown in Fig. 12 (a), the filled SPTC is burned through in the static airflow environment by the irradiation of the high-power CW laser. Several white columnar ablation residues with a size of about 20 μm are placed around the wall of the ablation hole. The composition of the white ablative residue formed by the oxidation of the silicone resin pyrolysis product corresponds to silicon dioxide.

The ablation morphology of the A-SPTC is different when the structure is subjected to the hypersonic airflow. As shown in Fig. 12 (b), due to the mechanical erosion effect, some cracks are produced in the surface of the ablation pit and the white silicon dioxide residue does not exist. Compared to that in the static air environment, the microstructure of the ablation residue shows narrower features. The size of the particles is about 2–3 μm. Energy dispersive analysis (EDS) and the carbon distribution of the main gradient of the ablation residue are shown in Fig. 13. The carbon is uniformly distributed at the surface of the ablation pit. The mixed carbon powders with particle diameter of 100–200 μm do not appear.

Comparisons of the results of thermogravimetric and DSC analyses between the filler material in the intact zone and the material around the ablation pit surface are shown in Fig. 14 and Fig. 15, respectively. The mass losses of the materials on the ablation pit surface in nitrogen and air atmospheres are only about 4 and 10 %, respectively, which is substantially lower than that of the intact filler material. This implies that some fractions of the pyrolysis products in the degradation layer are removed due to the aerodynamic force. In the hypersonic airflow environment, the aerodynamic force blows away the mixed carbon powder and inadequately pyrolytic polydimethylsiloxane, therefore, it rapidly accelerates the laser ablation process. Failure times of the unfilled SPTC and thermal insulation material-filled SPTC in the open-air environment are about 2–3 times higher than that under the hypersonic airflow.

5. Conclusions

The laser ablation behavior of four kinds of laser protection structures under the hypersonic airflow is experimentally investigated. The results show that the performance of the A-SPTC structures is substantially better than for the other three configurations. Failure times of the four investigated types of structures under the hypersonic airflow and in the static air environment increase in the following order: monolithic plate, unfilled SPTC, thermal insulation material-filled SPTC, and A-SPTC. The increment of the threshold of laser damage induced by the hypersonic airflow for the CW-laser induced damage threshold of the investigated structures are 69 %, 77 %, and 70 % for the plate, SPTC and I-SPTC, but less than 34 % for A-SPTC. The aerodynamic force accelerates the ablation rate of the ablation material by removing the mixed carbon powder and the inadequately pyrolytic polydimethylsiloxane in the strong airflow. With the increase of the ablation pit thickness, the static pressure near the right wall decreases, yielding an asymmetric ablation morphology.

CRediT authorship contribution statement

Wu Yuan: Conceptualization, Methodology, Writing – original draft. **Jiangtao Wang:** Data curation. **Ruixing Wang:** Software. **Zhe Wang:** Resources. **Hongwei Song:** Writing – review & editing, Funding acquisition. **Chenguang Huang:** Supervision.

Declaration of Competing Interest

The authors declare that they have no known competing financial interests or personal relationships that could have appeared to influence the work reported in this paper.

Data availability

Data will be made available on request.

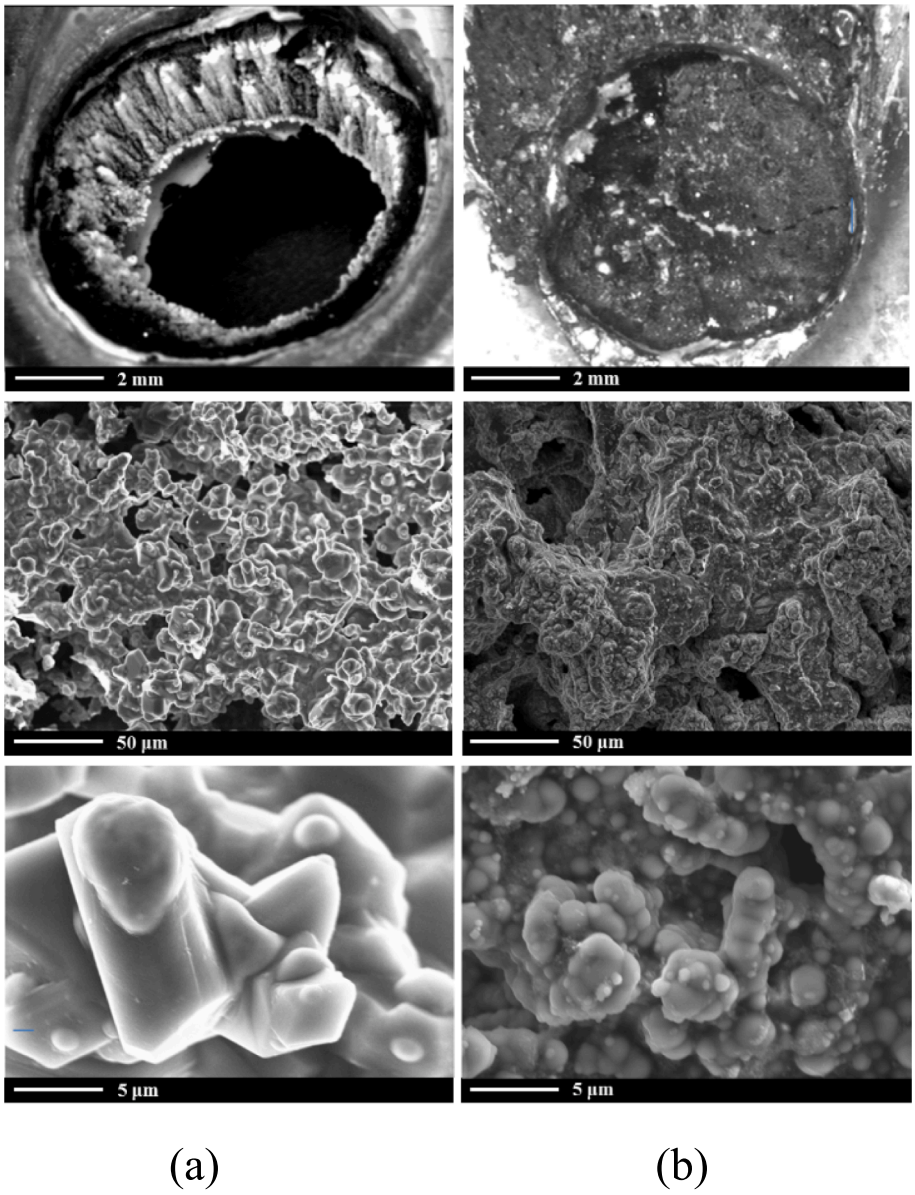

Fig. 12. Ablation morphologies for the ablative material-filled SPTC: (a) static environment, laser irradiation time 25 s, laser diameter 10 mm, laser power 1000 W, and (b) hypersonic wind tunnel with Mach 6.0, laser irradiation time 4 s, laser diameter 10 mm, laser power 1000 W.

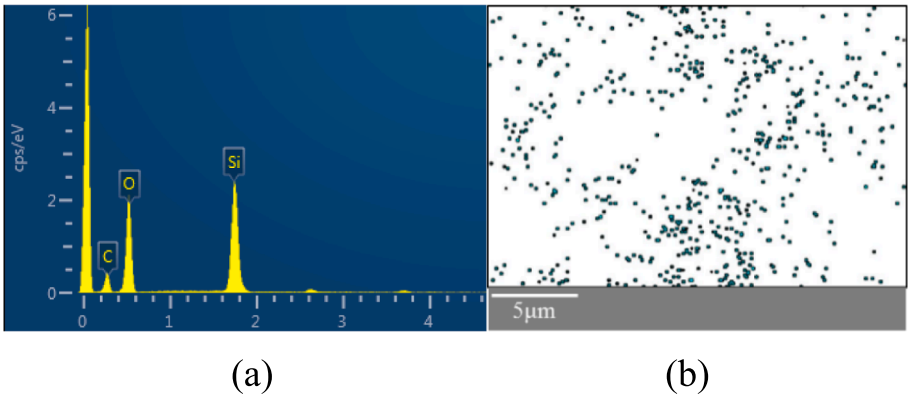

Fig. 13. Distribution of the main gradient of the ablation residue: (a) EDS analysis and (b) the carbon element distribution.

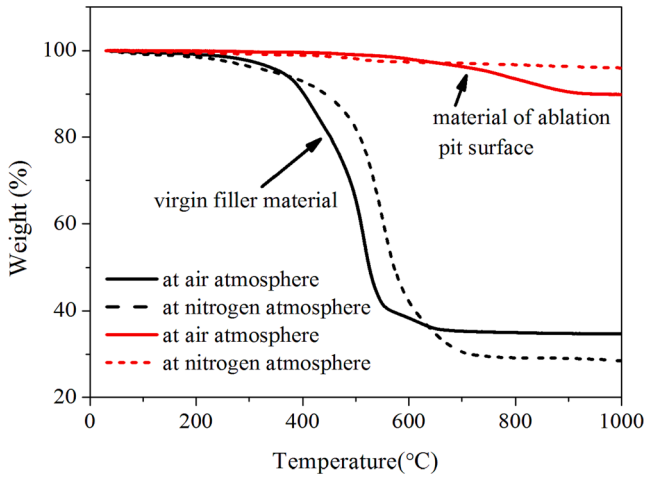

Fig. 14. Comparisons of the results of thermogravimetric analysis between the filler material in the intact zone and on the ablation pit surface.

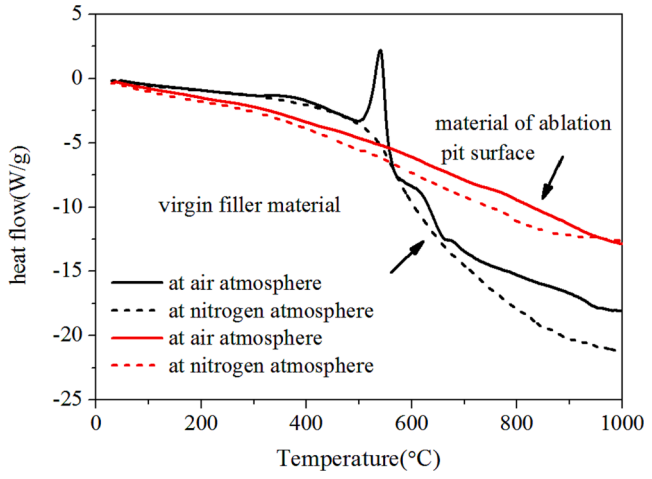

Fig. 15. Comparisons of the results of the DSC analysis between the filler material in the intact zone and the material on the ablation pit surface.

Acknowledgments

Financial supports from the National Natural Science Foundation of China (Grant Nos., 11972035, 11972033, 11332011, 11902201 and 12172229) are gratefully acknowledged.

References

[1] Milling RW. Laser defense and countermeasure system for aircraft; 1976.
[2] Branen KE, Castle GK, Mullen CK. Supersonic Vehicle Control Surface having a Thermally Protective. Coating 1973.
[3] Wang JT, Yuan W, Liu YW, Song HW, Huang CG. High-power laser resistance of filled sandwich panel with truss cores: Ablation mechanisms and numerical simulation. Compos Struct 2018;203:574–84.
[4] Yuan Wu, Wang J, Song H, Ma Te, Wu W, Li J, et al. High-power laser resistance of filled sandwich panel with truss core: An experimental study. Compos Struct 2018; 193:53–62.
[5] Cao X, Duan S, Liang J, Wen W, Fang D. Mechanical properties of an improved 3D-printed rhombic dodecahedron stainless steel lattice structure of variable cross section. Int J Mech Sci 2018;145:53–63.
[6] Kooistra GW, Deshpande VS, Wadley HNG. Compressive behavior of age hardenable tetrahedral lattice truss structures made from aluminium. Acta Mater 2004;52:4229–37.
[7] Li C, Lei H, Liu Y, Zhang X, Xiong J, Zhou H, et al. Crushing behavior of multi- layer metal lattice panel fabricated by selective laser melting. Int J Mech Sci 2018;145: 389–99.
[8] Cai X, Yang J, Hu G, Lu T. Sound absorption by acoustic microlattice with optimized pore configuration. J Acoust Soc Am 2018;144(2):EL138–43.
[9] Qiu X, Deshpande VS, Fleck NA. Finite element analysis of the dynamic response of clamped sandwich beams subject to shock loading. European Journal of Mechanics a-Solids 2003;22(6):801–14.
[10] Radford DD, Fleck NA, Deshpande VS. The response of clamped sandwich beams subjected to shock loading. Int J Impact Eng 2006;32(6):968–87.
[11] Yang H, Ma Li. Multi-stable mechanical metamaterials by elastic buckling instability. J Mater Sci 2019;54(4):3509–26.
[12] Yang J-S, Ma Li, Schmidt R, Qi Ge, Schröder K-U, Xiong J, et al. Hybrid lightweight composite pyramidal truss sandwich panels with high damping and stiffness efficiency. Compos Struct 2016;148:85–96.
[13] Ashby MF, Bréchet YJM. Designing hybrid materials. Acta Mater 2003;51(19): 5801–21.
[14] Yang H, Ma L. Multi-stable mechanical metamaterials with shape-reconfiguration and zero Poisson's ratio. Mater Des 2018;152:181–90.
[15] Johnson RL, Okeefe JD. Laser Burnthrough Time Reduction Due to Tangential Air-Flow - Interpolation Formula. Aiaa Journal 1974;12:1106–9.
[16] O'Keefe JD, Johnson RL. Laser Melt through Time Reduction Due to Aerodynamic Melt Removal. Aiaa Journal 1976;14(6):776–80.
[17] Crane KCA, Garnsworthy RK, Mathias LES. Ablation of Materials Subjected to Laser-Radiation and High-Speed Gas-Flows. J Appl Phys 1980;51(11):5954–61.
[18] Huang Y-H, Song H-W, Huang C-G. Heat Transfer and Mode Transition for Laser Ablation Subjected to Supersonic Airflow. Chin Phys Lett 2016;33(1):014201.
[19] Marineau EC, Schetz JA, Neel RE. Computational and Experimental Investigation of Supersonic Convection over a Laser-Heated Target. J Thermophys Heat Transfer 2009;23(3):502–12.
[20] Baumann SM, Hurst BE, Marciniak MA, Perram GP. Fiber laser heating and penetration of aluminum in shear flow. Opt Eng 2014;53(12):122510.
[21] Wang J, Ma Y, Liu Y, Yuan Wu, Song H, Huang C, et al. Experimental investigation on laser ablation of C/SiC composites subjected to supersonic airflow. Opt Laser Technol 2019;113:399–406.
[22] Robin JE, Nordin P. Reduction of Cw Laser Melt-through Times in Solid Materials by Transverse Gas-Flow. J Appl Phys 1975;46(6):2538–43.
[23] Robin JE, Nordin P. Enhancement of Cw Laser Melt-through of Opaque Solid Materials by Supersonic Transverse Gas-Flow. Appl Phys Lett 1975;26(6):289–92.
[24] Baek WK, Lee KC, An SI, Shin WS, Yoh JJ. Melt-through characteristics in continuous beam irradiation of flying metal samples in flow speeds up to 85 m/s. Opt Laser Technol 2013;45:250–5.
[25] Boley CD, Cutter KP, Fochs SN, Pax PH, Rotter MD, Rubenchik AM, et al. Interaction of a high-power laser beam with metal sheets. J Appl Phys 2010;107 (4):043106.
[26] Yuan W, Song HW, Lu LL, Huang CG. Effect of local damages on the buckling behaviour of pyramidal truss core sandwich panels. Compos Struct 2016;149: 271–8.
[27] Lawson SJ, Barakos GN. Review of numerical simulations for high-speed, turbulent cavity flows. Prog Aerosp Sci 2011;47(3):186–216.
[28] Larcheveque L, Sagaut P, Le TH, Comte P. Large-eddy simulation of a compressible flow in a three-dimensional open cavity at high Reynolds number. J Fluid Mech 2004;516:265–301.
[29] Sarohia V. Experimental Investigation of Oscillations in Flows over Shallow Cavities. Aiaa J 1977;15(7):984–91.